OPTIMIZATION DESIGN AND PERFORMANCE ANALYSIS OF A NOVEL BIONIC ROTARY CUTTER FOR A WEEDING MACHINE
/
新型除草机仿生旋转刀具的优化设计与性能分析

Wenjuan SHUN[2)], Jun GE*[1)], Kuan QIN[1)], Chengmao CAO[1)], Yan SUN[1)], Liangfei FANG[1)], Xu ZHU[1)], Junjie LU[1)], Weidong GAO[1)] [1]
[1)] School of Engineering, Anhui Agricultural University, Hefei, Anhui / China
[2)] College of Food and Nutrition, Anhui Agricultural University, Hefei, Anhui / China
Corresponding authors: Jun Ge; Tel: +8615077912067; E-mail: gejunahau@ahau.edu.cn
DOI: https://doi.org/10.35633/inmateh-76-82

Keywords: *weeding cutter, bionic, cicada nymph, DEM, three-direction resistance*

ABSTRACT
In a weeding machine, the weeder component determines overall working performance, while the weeding blade influences soil-cutting quality, weeding efficiency, resistance, and power consumption. In this paper, a bionic design for a weeding cutter inspired by the soil-cutting process of the cicada nymph has been proposed and the intent is to promote the performance of the bionic design. The weeding cutter introduced in this paper has been equipped with lightweight and simplified rotary robotic-machinery commonly utilized in hilly and mountainous areas. To assess the performance of the bio-mimetic weeding cutter during rotary, the forces in 3 directions (X, Y & Z) and the resistance torque have been investigated. An experimental platform with a 4 m long soil bin has been utilized for tests indoors. Meanwhile, the discrete element method (DEM) simulations with different conditions like the operated angle, the rotation speed, the forward velocity, and different cutting edges, have been carried out. Either the experimental result or the simulative result indicated that the bio-mimetic weeding blade ameliorated the performance of soil-cutting, energy consumption and weeding efficiency. Specifically, the bio-mimetic weeding blade exhibits a notable reduction of 14.19% in average torque and 14.95% in horizontal resistance compared to the traditional weeding blade. Finally, it could be found that the bionic rotary cutter proposed in this research could be a better choice for the weeder machine used in hilly and mountainous areas.

摘要
对于旋耕除草机械来说，除草刀是决定其工作性能的关键因素。具体而言，除草刀片决定了土壤切割的质量、除草效率、阻力和功耗。本文提出了一种受蝉若虫土壤切割过程启发的除草刀仿生设计，旨在提高除草刀的性能表现。本文介绍的除草机配备在丘陵山区常用的轻量化旋耕除草机械上。本研究为了评估仿生除草刀在旋转过程中的表现，研究了 3 个方向（X、Y 和 Z）的力和阻力扭矩。试验主要在 4 米长土槽平台中进行，之后，在参数标定的基础上进行了不同条件下的离散元法（DEM）模拟，主要变量包含操作角度、转速、前进速度和不同的切削刃。无论是土槽试验结果还是仿真模拟结果都表明，仿生除草刀片改善了土壤切割性能、能耗和除草效率。具体而言，与传统除草刀片相比，仿生除草刀片的平均扭矩显著降低了 14.19%，水平阻力显著降低了 14.95%。整体而言，本研究提出的仿生旋转切割器可能是丘陵山区除草机的更好选择。

INTRODUCTION
Peucedanum praeruptorum Dunn, known as Qianhu in Chinese, is the herb with high medicinal value in traditional Chinese medicine (*Chen et al., 2021*). In decades, the quality of Qian Hu has declined due to the excessive use of herbicides through chemical weeding (*Mayerová et al., 2018*). Generally speaking, there are three ways to remove the herbs in the field: manual weeding, chemical herbicide, and mechanical weeding. As a traditional method, weeding by hand has apparent limitations such as labor-intensive and time-consuming. Furthermore, the chemical way has the problem of herbicide residue which is strictly prohibited in the medical herb.

Wenjuan Shu, Stud. Eng.; Jun Ge, Lecturer PhD. Eng.; Xu Zhu, M.S. Stud. Eng.; Chengmao Cao, Prof. PhD. Eng.; Yan Sun, Assoc. Prof. M.S. Eng.; Liangfei Fang, Assoc. Prof. PhD. Eng.; Kuan Qin, Assoc. Prof. PhD. Eng.; Junjie Lu, M.S. Stud. Eng.; Weidong Gao, M.S. Stud. Eng.*

Different from the above two ways, mechanical weeding, serving as a chemical-free and environmentally friendly weed control method, has gained widespread recognition for effectively managing weed growth in various crops (*Richard et al., 2023; Fishkis & Koch, 2023; Liu, et al., 2023*).

Ning Qianhu, named after the Ningguo City (N 30°16′ - 30°47′, E 118°36′ - 119°24′), a hilly mountainous area in Anhui Province, China, is always cultivated in hilly mountainous regions. Due to the challenging terrain of steep mountains, large and medium-sized machinery is unsuitable for agricultural operations in this region. As a result, lightweight and simplified machinery is commonly employed *(Cao et al., 2023*). Micro-tillers are equipped with a maximum engine power of 6.5 kW which can effectively remove weeds in crop rows by the drove weeding wheels. The weeding wheel, a key component of micro-tillage machines, consists of multiple metal weeding blades transversely welded to the wheel hub. When a certain torque is applied, the weeding wheel tills the topsoil and removes weeds. However, traditional weeding wheels face challenges such as high resistance and power consumption during weeding operations. These issues lead to low weeding efficiency and high costs, which hinder the widespread adoption of agricultural mechanization *(Wang, et al., 2021)*. In recent years, researchers and scholars have focused on designing new weeders to enhance mechanization in hilly mountainous areas. Their efforts aim to optimize weeder performance, improve weeding efficiency, and reduce the cost of mechanical weeding. For instance, *Wang et al. (2011)* developed a novel 3ZS-150 tillage weeder for weed control in paddy fields. That innovative machine enables simultaneous weeding between rows and seedlings. The study conducted a systematic analysis of the machine's structure and working principles, introducing a novel design of the weeding spring tooth for effective removal of intra-row weeds and inter-row cultivation. Furthermore, *Wang et al. (2017)* developed a simplified 3SCJ-2 paddy inter-row weeder, focusing on a more comprehensive analysis of the structural design and power distribution of a small-scale weeding machine. The study established a mechanical model of the weeding wheel, determining essential working and structural parameters. These efforts resulted in a lightweight and straightforward weeding machine design that ensures low power consumption and high efficiency. The optimization of the geometric structure of the rotary cutter, along with the relevant operating and structural parameters, has been a prominent focus of research within the context of previous studies on rotary cultivator design. For instance, *Matin, Fielke, and Desbiolles (2014)* have explored the impact of the geometric shape and operating speed of the rotary cultivator on torque, energy consumption, and the soil cutting and throwing process. The research has investigated the interaction between the cutting edges of the blades and the soil to determine the optimal design for the rotary cultivator. Efforts to optimize the geometric structure of the weeding wheel and its associated parameters are crucial for enhancing the overall performance and efficiency of the weeding process *(Matin et al., 2014, 2015, 2020).*

In summary, to address the challenge of high resistance in weeding blades used in micro-tillage weeders operating in hilly mountainous areas, this paper presents a novel bionic rotary weeding cutter inspired by the serrated characteristics of the forelimbs of nymphal cicadas, which holds promise for improving the performance of weeding wheels in micro-tillage weeders. Furthermore, a mechanical model of soil-weeding cutter interaction was established to further study the resistance change of the rotary cutter in the process of cutting soil.

MATERIALS AND METHODS

This paper proposed a bionic design approach for developing weeders suitable for hilly mountainous areas. Figure 1 illustrates the robotic micro-tillage weeder machine specifically designed for the Ning Qianhu. The machine contains a separated roll-cutting weeding wheel for inter-row weeding. During the weeding process, the weeding blades shear and break the topsoil, effectively removing the weeds embedded in the soil. Therefore, the soil and weeds are propelled backwards with the weeding blades rotating *(Tian et al., 2022)*.

Extracting and fitting the serrated structure

Samples of *Cicadas nymphs* were collected from Anhui, China, to study the excavating process, as shown in Figure 1. The tibia continuously opened, retracted, and drove the serrated structure, effectively cutting through the sediment *(Smith & Hasiotis, 2008)*. These serrations exhibited a cutting angle that extended beyond the friction angle, providing a slip-cutting effect. That characteristic was crucial for achieving efficient cutting and reducing cutting resistance during the emergence of *Cicadas nymphs* and it shares many similarities with rotary tillage tools in terms of soil cutting *(Chang et al., 2016)*. Enlarged photographs of the serrated structures of *Cicada Nymphs* were captured using an electron microscope. To enhance the quality of the images and reduce noise, a combination of Gaussian filtering and the Laplace operator was applied as a preprocessing step. Subsequently, image binarization was performed, followed by the utilization of the Canny

edge detection operator, which enabled accurate positioning and robust resistance to interference. Finally, the Find function was employed to extract the contour pixel coordinates. The results of the contour extraction are illustrated in Fig. 2. A total of 3969-pixel coordinate points were extracted in this figure. The contour curves of the cicada's saw-tooth structure exhibited four distinct curves, namely A, B, C, and D. Among those curves, in terms of manufacture and curvature, curve D was more feasible and suitable for the bionic saw-tooth profile in this study. Subsequently, the accorded dimensions for manufacturing the bio-mimetic blade teeth are shown in Figure 3 and manufactured products are shown in Fig. 4.

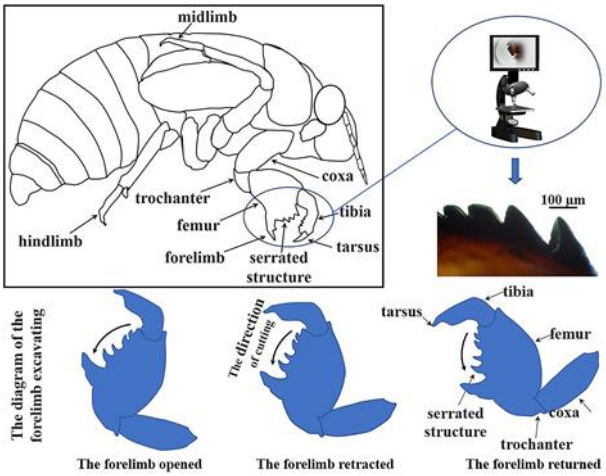

Fig. 1 – Serrated structure of the cicada nymph

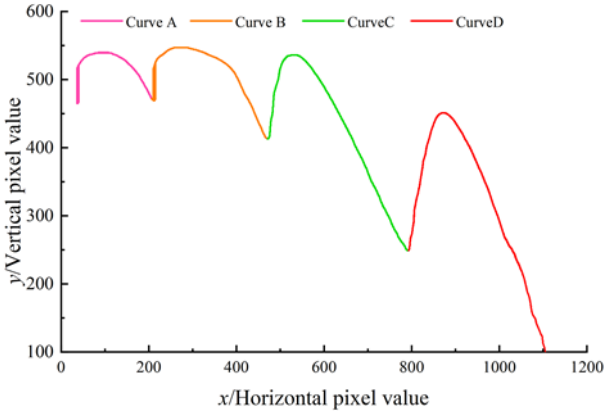

Fig. 2 – Pixel chart for the saw-tooth profile on forelimbs of the cicada nymph

No.	Items	Unit	Value
1	t	mm	6.3
2	h	mm	4.6
3	ζ	degree	55
4	λ	degree	55
5	φ	degree	20

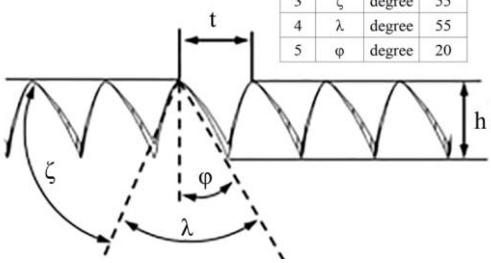

Note: t, distance between teeth; h, teeth height; ζ, teeth tilted angle with horizontal line; λ, angle of the teeth profile; φ, angle between the right side of teeth profile and vertical line

Fig. 3 – Teeth dimensions of the bio-mimetic weeding blade

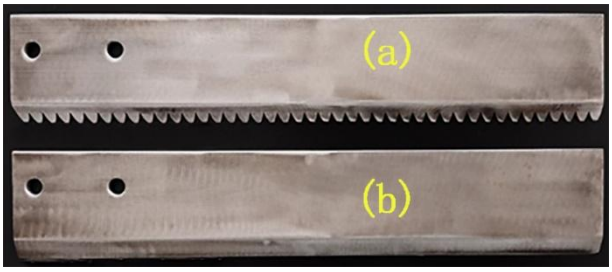

Fig. 4 – Physical picture of bio-mimetic (a) and traditional weeding blade (b)

Weeding blade parameter and resistance analysis

The mounted angle of the blade *α*, defined as the angle between the tangent to the radius of rotation and the blade, is a significant parameter for soil entry and exit, as illustrated in Fig. 5. When the blade enters the soil, the entry angle *β* should be noted; it varies with the mounted angle α, as shown in Fig. 5(a) and 5(c). Fig. 5(a) is a normal situation whereas Fig. 5(c) has a perpendicular *β*. In Fig. 5(a), the contacted F_N has been decomposed into F_{Nx} in the tangent direction and F_{Ny} in the normal direction. F_{Nx} is mainly affected by the angle *β*, while F_{Ny} is relevant to the weight and the slip ratio of the weeder machine. The relationship between F_N, F_{Nx} and F_{Nxy} could be expressed as follows:

$$\begin{cases} F_{Nx} = F_N \cos\beta \\ F_{Ny} = F_N \sin\beta \end{cases} \quad (1)$$

The maximum weeding depth is h, the blade width is L, and the trajectory radii of the blade top and end are R_1 and R_2. In this study, the blade width L, depth h, and R_1 were 40 mm, 40 mm and 123 mm, respectively. Meanwhile, the entry angle *β* was set at 90° for a minimum penetration resistance. The following Eqs. (2), (3) were then obtained:

$$\frac{1}{2} R_1 + L + h \ = R_1 + L \times \sin\alpha \quad (2)$$

$$\alpha = \sin^{-1}\frac{L + h - \frac{1}{2}R_1}{L} \tag{3}$$

A microscopic view of the forces acting on a soil particle is shown in Figure 5(b). The abscissa *x'* is parallel to the blade surface, while the longitudinal axis *y'* passes through the center of the particle and is perpendicular to *x'*. The force F on the soil particle is the resultant of the frictional force and the support force; F_a and F_n are the components of F in the directions of *x'* and *y'*, respectively. F_a can be calculated using Eq. (4).

$$F_a = \cos\alpha \;\; F \tag{4}$$

Generally speaking, F_a is affected by the angle *α* of the weeding blades *(Zhang et al., 2022)*. Based on Eq. (4), a smaller α makes a greater F_a. On the other hand, it means greater soil adhesion and power consumption as the blade moves. Therefore, an appropriate angle α should be assigned in the first place.

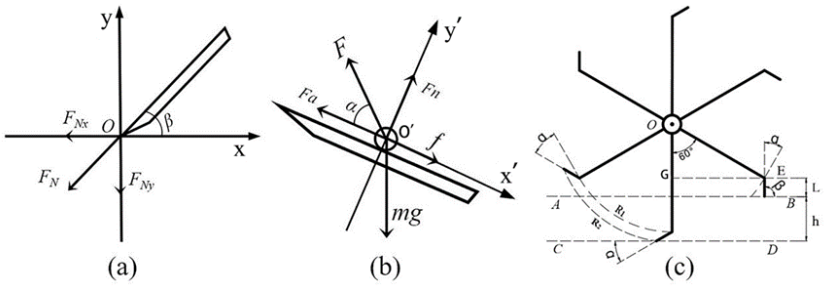

Fig. 5 – Mechanics analysis for soil-blade interaction system

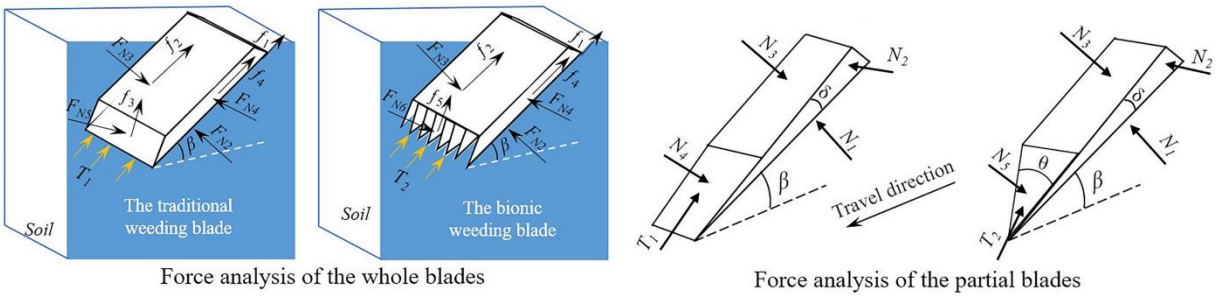

Fig. 6 – Respective mechanic analysis for traditional and bionic weeding blade

Figure 6 diagrammatically compares the forces generated by traditional and bionic weeding blades as they are contacting with soil, respectively. To compare the resistance of the two blades, both the bionic blade and traditional blades were divided into several units. The bionic blade edge can be approximated as a triangular shape that serves as the unique profile of the bionic saw-tooth. Figure 6 intuitively reflects the difference in force between these two blades. In the figure, N_1, N_2, N_3, N_4 and N_5 were pressures acting on different faces of the blades' element. T_1, T_2 were the pure cutting resistances, and *θ* represented the sharpness angle of the blade head. According to the cutting model of Kostritsyn *(Zeng, 1995)*, the forces in Figure 6 could be expressed as follows:

$$P_1 = \cos\delta\left(\frac{M_1\cos\beta}{\tan(\delta+\beta)} + M_1\cos\beta\,\mu\right) + \cos\delta\left(\frac{N_3}{\tan\beta} + N_3\mu + 2N_2\mu\right) + \frac{mse}{cos(\delta + tan^{-1}\mu)}S_1\mu + kb_1 \tag{5}$$

$$P_2 = \cos\delta\left(\frac{M_1\cos\beta}{\tan(\delta+\beta)} + M_1\cos\beta\,\mu\right) + \cos\delta\left(\frac{N_3}{\tan\beta} + N_3\mu + 2N_2\mu\right) + \frac{mse}{cos(\delta + tan^{-1}\mu)}S_2\mu + kb_2 \tag{6}$$

where:

P_1 was the resistance of the traditional blade along the direction of the blade edge.

P_2 was the resistance of the bionic blade along the direction of the blade edge.

According to Eq. 5 and Eq. 6, the resistance of the bionic blade should be less than that of the traditional blade due to $b_1 > b_2$ and $S_1 > S_2$.

Calibration of DEM parameters

Soil parameters determined the accuracy of DEM simulation *(Wu et al., 2021)*. In the field, the five-point sampling method was employed to assess the density and water content of the soil within the 0-250 mm depth range. As a result, the tested soil has a density of 1.51 g·cm^{-3} and water content of 18.15%. The vibratory sieving method revealed the distribution of soil particle sizes: the sand particles were more than 20% and the powder particles were less than 40%. According to the Chinese Soil Texture Classification, the sandy loam could be an appropriate result for the test soil. Moreover, the repose angle of soil, shown in Figure 7(a), (b) and (c), yielded an average value of 33.7°.

Table 1

Parameters utilized in DEM simulation

Type of parameter	Values	Type of parameter	Values
Soil particle diameter (mm)	4	Soil-soil static friction coefficient	0.6
Soil density (g·cm^{-3})	1.51	Soil-soil rolling friction coefficient	0.3
Soil shear modulus	1e+06	Soil-soil restitution coefficient	0.5
Soil Poisson's ratio	0.35	JKR with surface energy (J·m^{-2})	1
Weeding blades density (g·cm^{-3})	7.89	Soil- blades friction coefficient	0.5
Weeding blades shear modulus (Pa)	2.1e+11	Soil- blades rolling friction coefficient	0.05
Weeding blades Poisson's ratio	0.3	Soil- blades restitution coefficient	0.5

Based on the field tests, the calibration process/tests should be replicated in the DEM simulations to try the parameters of soil particles. Because of the cohesive force between soil particles, the Hertz-Mindlin model with the JKR soil contact model was chosen to simulate the binding and agglomeration forces between the soil particles *(Zhang et al., 2022, 2023)*. As Figure 7(d) shows, there was a cylinder and a circular plate to implement the repose angle test in the DEM simulation. In terms of the calibration result, the calibrated parameters of the soil particles used in DEM tests, such as the soil collision coefficient, soil rolling friction coefficient, soil static friction coefficient, and JKR surface energy, are shown in Table 1.

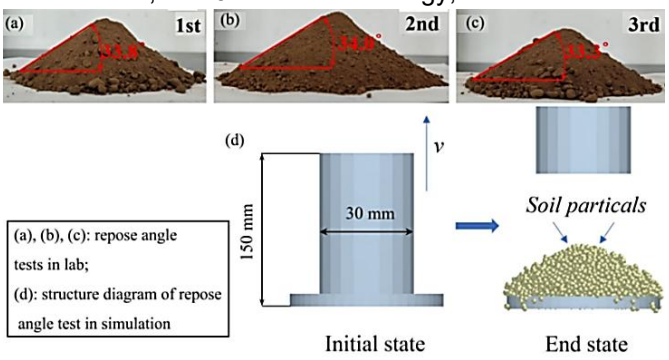

Fig. 7 – Repose angle test in lab and simulation for parameters calibration

Condition of Soil bin test

Due to the relatively stable performance of repeated experiments, the soil bin test is widely used for soil-related studies. In this study, a soil bin experiment was also conducted for comparison with the DEM simulation. In the soil bin test, both the traditional and bionic weeding wheels were represented by a single blade.

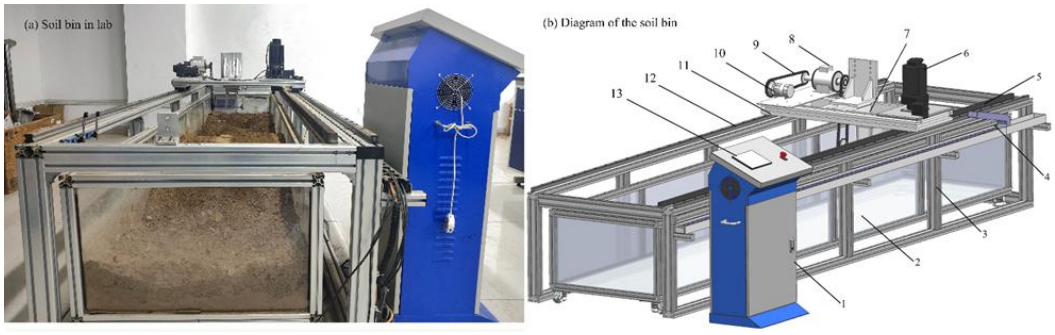

Fig. 8 – Experimental site picture and structural diagram of the soil bin

1. Electrical control box; 2. Soil tank; 3. Body frame; 4. Wire trays; 5. Forward guides (left side); 6. Electric motor for forward motion; 7. Three-direction force sensor; 8. Torque transducer; 9. Chain; 10. Electric motor for blade drive; 11. Moving platform; 12. Forward guides (right side); 13. Human–machine interface

As Fig. 8 shows, the experimental device contains thirteen main parts and the details have been noted below the figure, respectively. The soil bin has a length of 4 m, a width of 1 m and a depth of 0.8 m. Experimental soil, whose properties were stated in the last section, was collected from the Ning Qianhu plantation area. The moving platform (11 in Fig. 8(b)) could be moved with speeds ranging from 0 to 1.5 m·s-1 along the guiding chute. The three-direction forces sensor (7 in Fig.8(b)) was positioned beneath the movement mechanism. The rotation of weeding blade could be controlled by a speed controller and adjacent to the soil bin, a control cabinet was installed, enabling the setting of forward speed and displacement of the test device, as well as a real-time data display. The settings and parameters are shown in Table 2.

Table 2

The values of the test parameters

Type of parameter	values	Type of parameter	values
Forward speed /(m·s^{-1})	0.3	Blade width /(mm)	40
Rotational speed /(rpm)	150	Blade thickness /(mm)	3
Test length /(mm)	1000	Weeding depth /(mm)	40
Mass of the weeding blade /(g)	220	Weeding width /(mm)	217

RESULTS AND DISCUSSION

Simulation tests7

As mentioned above, the torque and three-direction forces were significant factors in indicating resistance when the weeding blade contacted the soil. Therefore, the DEM simulation of traditional and bionic blades focused on the comparison of the torque and three-direction forces by these two blades, too.

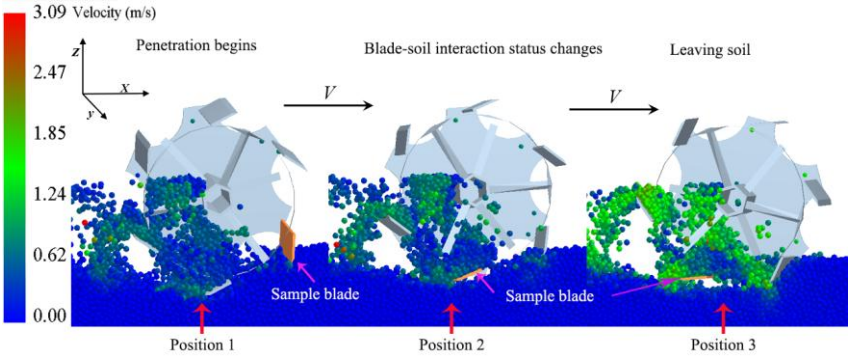

Fig. 9 – Blade-soil interaction and the movement of soil particles at different positions during weeder rotation in the DEM simulation

The blade interacted with the soil in different states during wheel rotation. As illustrated in Fig. 9, position 1 corresponds to the sample blade just penetrating the soil surface; position 2 represents the blade at the trough point of the trajectory curve; and position 3 shows the blade beginning to throw the soil away. Based on Fig. 9, soil particle disturbance increased from a mild degree at position 1 to the highest level at position 3. Hereinafter, the traditional weeding blade and the biomimetic blade are compared in terms of torque and three-directional forces based on the experimental results.

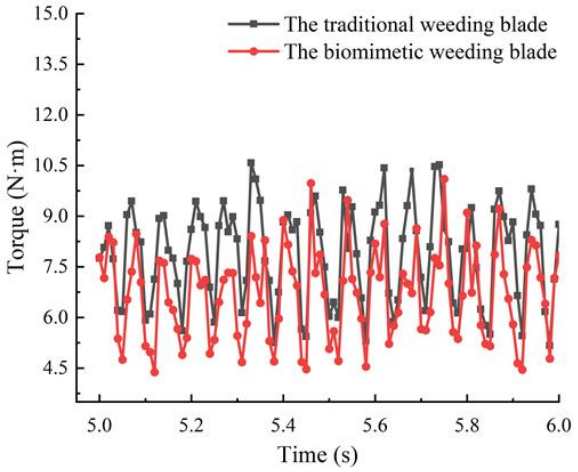

Fig. 10 – Difference between traditional and biomimetic weeding blades in torque on one blade during the blade touch with soil

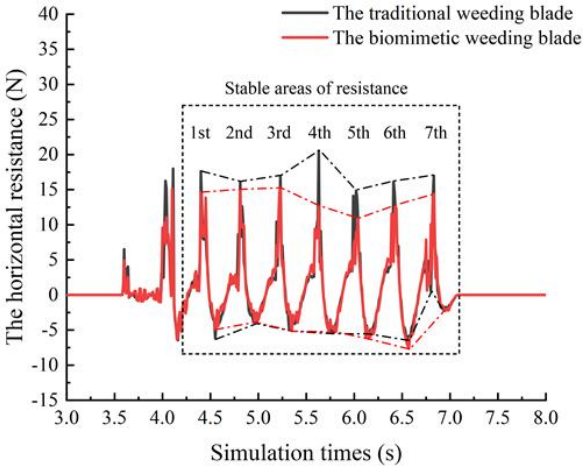

Fig. 11 – Horizontal resistance of the sample blade during the whole process in simulation

Figure 10 shows the variation in torque for the two types of weed wheels. As the figure shows, both the biomimetic weeding wheel and the traditional weeding wheel exhibited regular fluctuations. However, the biomimetic weeding wheel required less torque than the traditional weeding wheel for rotating the wheel. The results indicated that the average torque required for the traditional weed wheel was 7.89 N·m. In comparison, the biomimetic weeding blade exhibited a lower average torque of 6.71 N·m, representing a reduction of 14.95%. To facilitate a clear observation of the force variations during the simulation, the direction of the three-direction resistance on the weeding wheel is defined as follows: horizontal along the X-axis (aligned with the forward direction), vertical along the Z-axis, and lateral along the Y-axis.

As Figure 11 shows, the horizontal resistance of the weeding blade aligns with the forward direction, resulting in a positive horizontal resistance. Based on the previous analysis, the horizontal resistance of the weeding blade primarily arises from the shear resistance and friction of the soil. The variation in horizontal resistance can be observed for the two different weeding blades in the soil. At the moment of 5.05 s, the weeding blade contacts with the soil. As the depth of the weeding blade increases, the amount of soil adjacent to the weeding blade also increases, and it caused the angle between the weeding blade and the horizontal surface to be decreased to an acute angle. Consequently, the soil pressure, shear resistance, and frictional force against the weeding blade gradually increased, resulting in a progressive rise in horizontal resistance. This horizontal resistance represents the resistance encountered by the weeding blade during soil penetration and primarily depends on the depth of penetration. The graph indicates that the peak positive horizontal resistance occurred at 5.09 s, corresponding to the moment when the weeding blade reaches its maximum depth. Comparing the peak resistance values of the different weeding blades in simulation, it can be found that the peak resistance for the traditional weeding blade during soil penetration ranges from 12.27 N to 20.50 N, while for the biomimetic weeding blade, the peak resistance ranges from 9.31 N to 13.89 N.

The variation of horizontal force during a full rotation of a blade with the wheel is shown in Fig. 12.

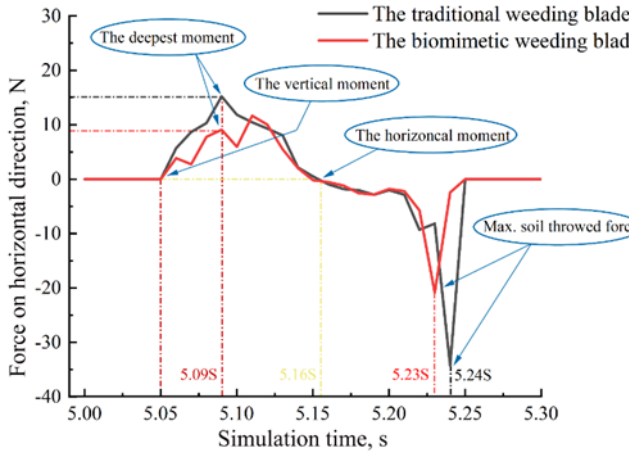

Fig. 12 – Horizontal resistance of blades over time

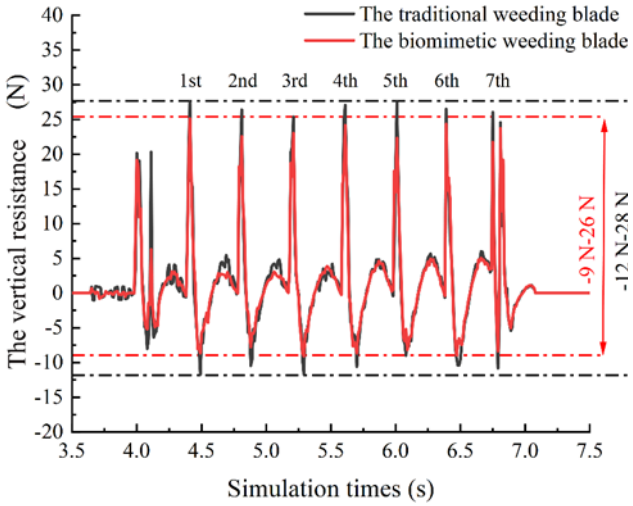

Fig. 13 – Vertical resistance of blades

During the simulation, the weeding blade was moved at a speed of 0.3 m·s-1 and rotated at 150 rpm, resulting in ten cycles of entering and leaving the ground. As illustrated in Figure 12, starting from the 3.46 s mark, the weeding blade entered the soil every 0.4 s, resulting in ten successive periodic variations. However, only seven of these variations in resistance were continuous. By calculating the average horizontal resistance value, it was found that the traditional blades had an average value of 8.17 N, while the bionic blades had an average value of 7.01 N. As a result, the bionic blades showed a reduction in horizontal resistance of approximately 14.19%. After reaching the peak resistance value, the angle between the blade and the horizontal surface gradually decreases. Consequently, the soil pressure in the horizontal component also gradually decreases, leading to a decrease in the horizontal resistance until it reaches 0 N. Meanwhile, the force in the vertical direction also reached its peak value. The variation in vertical resistance over the simulation time is shown in Fig. 13.

As depicted in Fig. 13, at this stage, the vertical resistance observed is the result of the weeding blades throwing off the soil, as the angle between the weeding blade and the horizontal surface becomes negative. Both types of resistance are influenced by similar forces, primarily the shear resistance of the soil, gravity, and

friction. Consequently, they exhibit similar fluctuations, increasing and decreasing in a synchronized manner. In addition, positive values indicate the reaction force of the soil on the blade, while negative values represent the resistance caused by the gravity and adhesion of the soil. The average vertical resistance surpasses the average horizontal resistance, highlighting that the primary resistance faced by the weeding wheel during the weeding process is vertical. The maximum vertical force recorded for the traditional weeding blade was 31.06 N, while the bionic weeding blade was 35.58 N. Additionally, the average vertical resistance in the forward direction was 11.90 N for the traditional blade and 12.75 N for the bionic blade, while the vertical resistance in the backward direction was 8.7 N.

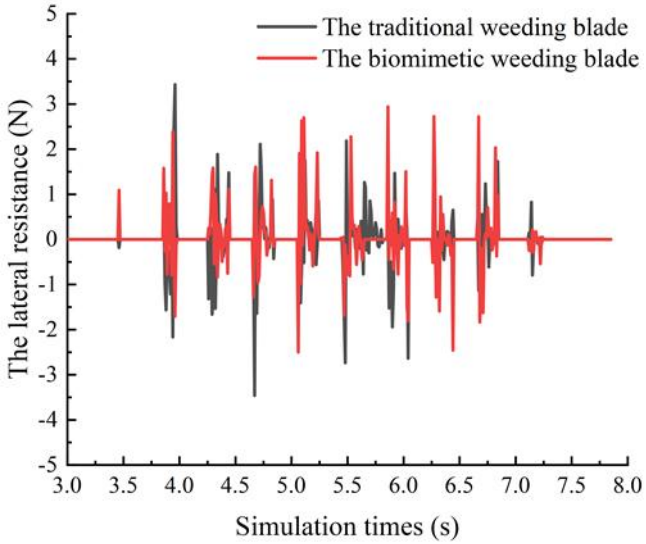

Fig. 14 – Lateral resistance of the blades

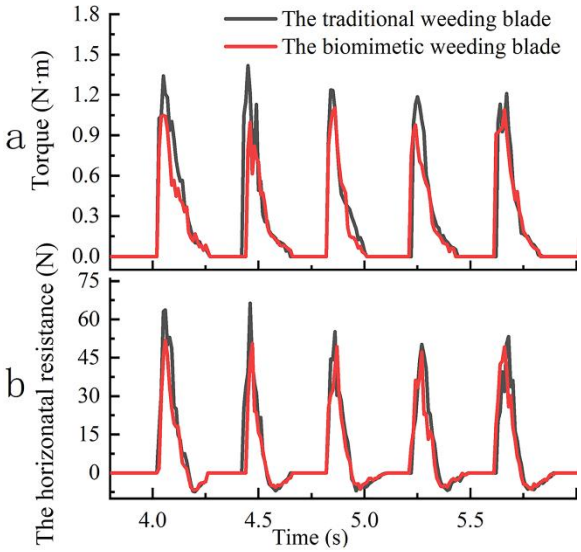

Fig.15 – Soil bin test result curve

Fig. 14 displays the lateral force diagram of the weeding blade. It is evident that lateral resistance also exhibits ten-fold variations. However, the maximum lateral resistance for the traditional weeding blade was 3.46 N, whereas, for the biomimetic weeding blade, it was 3.39 N. The average lateral resistance for the traditional weeding blade was 0.582 N, and for the bionic weeding blade, it was 0.585 N. The lateral resistance of the weeding blade primarily arises from the small amount of soil present and the friction and lateral pressure exerted by the soil during blade movement. Consequently, the lateral resistance values are small and remain consistent.

Overall, the weeding blade experiences two main types of resistance during operation: vertical resistance and horizontal resistance. The magnitude of both depends on the depth of blade penetration and the angle formed with the horizontal surface, with deeper penetration and smaller angles resulting in increased resistance. When comparing the two blade types, the average horizontal resistance of the biomimetic weeding blade was 14.19% lower than that of the traditional blade. The difference in vertical resistance was relatively small, at 11.90 N and 12.75 N, respectively.

Soil bin experiment

During weed control, the performance of different weed blades can be evaluated by comparing their torque. The torque of a weed blade indicates the amount of power required and is directly proportional to the resistance encountered during penetration.

Fig. 15(a) shows the soil bin test torque results comparing the traditional weeding blade and the biomimetic weeding blade. The eight obvious fluctuations in Figure 15(a) represent the eight times that the weeding blade cut the soil. Each torque fluctuation has a sudden rise stage, after reaching the peak, there is a fluctuating decline to 0 N. On the whole, individual weeding blade torque consumption was low on average, and the bionic weeding blade was always lower than the traditional weeding blade. The simulation of the weed blade revealed a significant difference between the two types of blades, primarily in terms of horizontal resistance, while the vertical and lateral resistances were similar to each other. Fig. 15(b) presents the variation in horizontal resistance between the two blades. In Fig. 15(b), the change in horizontal resistance follows the same trend as the change in torque in Fig. 15(a).

As shown in Table 3, the average torque value for the traditional weeding blade was 0.2097 N·m, while the average torque value for the biomimetic weeding blade was 0.1782 N·m, representing a 15.02% reduction in average torque. The total torque applied to the weeding wheel is the sum of the torques exerted by each blade on the weeding wheel. Therefore, the biomimetic weeding blade performs better in terms of average torque.

Summing up, it is known that the average horizontal resistance of the bionic weeding blade was reduced by 14.99% compared to the traditional weeding blade and 15.02% in average torque. Thus, the bionic weeding blade outperforms the traditional weeding blade in terms of both torque and resistance reduction. Additionally, in terms of horizontal resistance reduction and torque reduction, the results of the soil bin test and simulation experiment were consistent and the error was within the controllable range.

Table 3

The test result of torque and horizontal resistance in the soil bin

No. of test	Average horizontal resistance of traditional weeding blade /N	Average horizontal resistance of biomimetic weeding blade / N	Average torque of traditional weeding blade /N·m	Average torque of biomimetic weeding blade / N·m
The 1st	15.85 N	13.54 N	0.2033 N·m	0.1747 N·m
The 2nd	15.17 N	12.96 N	0.2056 N·m	0.1760 N·m
The 3rd	17.68 N	14.90 N	0.2202 N·m	0.1840 N·m
Average values	16.24 N	13.80 N	0.2097 N·m	0.1782 N·m

CONCLUSIONS

The forelimbs of the cicada nymphs were observed and photographed using a microscope to capture its sawtooth structure. The image processing technique was employed to extract the contour curve of the sawtooth structure, which was then fitted by using Origin2021. The fitted function underwent analysis of its second-order derivatives and curvature. The resulting contour curve, referred to as D, was chosen as the basis for the bionic sawtooth. Subsequently, a 3D model of the bionic weeding blade was designed.

The basic parameters of the soil in Ningguo City's Qianhu plantation were determined. To simulate the sandy loam soil found in Ningguo City, situated in the hilly mountainous region of southern Anhui, a simulation model was established. The DEM simulation employed the Hertz-Mindlin contact model with JKR as the soil contact model.

Weeding blade simulation tests were conducted to compare the performance of the bionic weeding blade and the traditional weeding blade. The simulations revealed that the bionic weeding blade required 14.95% less torque than the traditional weeding blade. The difference between the two types of blades depended on the depth of penetration into the soil and the angle between the blades and the horizontal plane. Deeper penetration and smaller angles resulted in increased horizontal and vertical resistance. The bionic weeding blade demonstrated an average reduction of 14.19% in horizontal resistance compared to the traditional weeding blade under specific conditions.

Comparative soil trough tests were performed using the weed blade to further evaluate its performance. The results of these tests confirmed the trend observed in the simulation tests. The average torque applied to the bionic weeding blade was lower than that of the traditional weeding blade, showing a reduction of 15.02%. The horizontal resistance showed a reduction of 14.99%.

ACKNOWLEDGEMENT

The authors were supported by Anhui Provincial Natural Science Foundation (2308085ME160).

REFERENCES

[1] Chang, Z., Liu, W., Tong, J., Guo, L., Xie, H., Yang, X., Mu, H., Chen, D. (2016). Design and experiments of biomimetic stubble cutter. *Journal of Bionic Engineering*, Vol.13, Iss.2, pp. 335-343, Jilin/China.

[2] Chen, F., Tu, L., Liu, D., Ma, J., Luo, Y. (2021). Chemical constituents from the roots of *Peucedanum praeruptorum* Dunn and their chemotaxonomic significance. *Biochemical Systematics and Ecology,* Vol. 99, No. 104355, Nanchang/China.

[3] Cao, C., Xiang, W., Luo, K., Wu Z., Zhang, X., Qin, K. (2023). Design and experiment of *Radix Peucedani* weeding machine separating weeds and soil with combination of throwing and pushing (抛推组合式草土分离前胡除草机设计与试验). *Transactions of the Chinese Society for Agricultural Machinery*, Vol. 54, Iss. 03, pp. 106-114, Hefei/China.

[4] Fishkis, O., Koch, H. (2023). Effect of mechanical weeding on soil erosion and earthworm abundance in sugar beet (Beta vulgaris L.). *Soil and Tillage Research*. Vol. 225, No.105548, Germany.
[5] Liu, C., Yang, K., Chen, Y., Gong, H., Feng, X., Tang, Z., Fu, D., Qi, L. (2023). Benefits of mechanical weeding for weed control, rice growth characteristics and yield in paddy fields. *Field Crops Research*, Vol. 293, No. 108852, Guangzhou/China.
[6] Matin, M.A., Fielke, J.M., Desbiolles, J. (2014). Furrow parameters in rotary strip-tillage: Effect of blade geometry and rotary speed. *Biosystems Engineering*, Vol. 118, pp. 7-15, Australia.
[7] Matin, M.A., Fielke, J.M., Desbiolles, J. (2015). Torque and energy characteristics for strip-tillage cultivation when cutting furrows using three designs of rotary blade. *Biosystems Engineering*, Vol. 129, pp. 329-340, Australia.
[8] Mayerová, M., Madaras, M., Soukup, J. (2018). Effect of chemical weed control on crop yields in different crop rotations in a long-term field trial. *Crop Protection*, Vol. 114, pp. 215-222, Czech.
[9] Matin, M.A., Hossain, M.I., Gathala, M.K., Timsina, J., Krupnik, T.J. (2020). Optimal design and setting of rotary strip-tiller blades to intensify dry season cropping in Asian wet clay soil conditions. *Soil and Tillage Research*, Vol. 207, No. 104854, Bangladesh.
[10] Richard, D., Leimbrock-Rosch, L., Keßler, S., Stoll, E., Zimmer, S. (2023). Soybean Yield Response to Different Mechanical Weed Control Methods in Organic Agriculture in Luxembourg. *SSRN Electronic Journal*, Vol. 147, No. 126842, Germany.
[11] Smith, J.J., Hasiotis, S.T. (2008). Traces and burrowing behaviors of the cicada nymph Cicadetta calliope: Neoichnology and paleoecological significance of extant soil-dwelling insects. *Society for Sedimentary Geology*, Vol. 23, pp. 503-513, USA.
[12] Wang, J., Niu, C., Zhang, C., Wei, C., Chen, Z. (2011). Design and experiment of 3ZS-150 paddy weeding-cultivating machine (3ZS-150 型水稻中耕除草机设计与试验). *Transactions of the Chinese Society for Agricultural Machinery*, Vol. 42, Iss. 02, pp. 75-79, Harbin/China.
[13] Wang, J., Wang, J., Yan, D., Tang, H., Zhou, W. (2017). Design and experiment of 3SCJ-2 type row weeding machine for paddy field (3SCJ-2 型水田行间除草机设计与试验). *Transactions of the Chinese Society for Agricultural Machinery*, Vol.48,Iss. 06, pp. 71-78, Harbin/China.
[14] Wu, Z., Wang, X., Liu, D., Xie, F., Ashwehmbom, L.G., Zhang, Z., Tang, Q. (2021). Calibration of discrete element parameters and experimental verification for modelling subsurface soils. *Biosystems Engineering*, Vol. 212, pp. 215-227, Hunan/China.
[15] Wang, J., Ma, X., Tang, H., Tang, H., Wang, Q., Wu, Y., Zhang, Z. (2021). Design and experiment of curved-tooth oblique type inter-row weeding device for paddy field (曲面轮齿斜置式稻田行间除草装置设计与试验). *Transactions of the Chinese Society for Agricultural Machinery*, Vol. 52, Iss. 04, pp.91-100, Harbin/China.
[16] Zeng, D. (1995). Soil Machine Dynamics. China: *Bejing Science and Technology Publishing Co.,Ltd*, pp. 414-438, Beijing/China.
[17] Zhang, Y., Tian, L., Cao, C., Zhu, C., Qin, K., Ge, J. (2022). Optimization and validation of blade parameters for inter-row weeding wheel in paddy fields. *Frontiers in Plant Science*, Vol. 13, No. 1003471, Hefei/China.
[18] Zhang, Z., Xue, H., Wang, Y., Xie, K., Deng, Y. (2022). Design and experiment Panax notoginseng bionic excavating shovel based on EDEM (基于离散元法的三七仿生挖掘铲设计与试验). *Transactions of the Chinese Society for Agricultural Machinery*, Vol. 53, Iss. 5, pp. 100-111, Kunming/China.
[19] Zhang, S., Zhao, H., Wang, X., Dong, J., Zhao, P., Yang, F., Chen, X., Liu, F., Huang, Y. (2023). Discrete element modeling and shear properties of the maize stubble-soil complex. *Comput. Electron. Agric.*, Vol. 204, No.107519, Yangling/China.